Optimal Control of Intermodulation Distortion in Hybrid Fiber-Coaxial CATV Systems

Gary D. Alley, *Senior Member, IEEE*, and Yen Long Kuo, *Fellow, IEEE*

***Abstract*— The distortion optimization in a phase-controlled hybrid fiber coaxial (HFC) CATV system is presented both in the frequency domain and in the time domain. A general quadratic-phase relationship of the National Television System Community (NTSC) video carriers has been used as the basis for minimizing the peak/rms ratio of the broad-band signal as well as the second- and third-order intermodulation distortion products. Emphasis is placed on distortion products which fall outside the band occupied by the NTSC signals and thus degrade digital performance. An experimental phase-controlled coherent HRC CATV system consisting of 81 live video channels and four 64 quadrature amplitude modulation (QAM) digital channels has been used to demonstrate the advantages of an optimal phase-controlled headend over traditional systems.**

I. Introduction

The performance of hybrid fiber coaxial (HFC) systems, which carry a mixture of National Television System Community (NTSC) video and digitally modulated signals, is limited by intermodulation distortion due to the total system payload. Nonlinearities in the system cause the digital signals, in conjunction with the NTSC video signals, to produce broad-band intermodulation noise which falls in the NTSC video spectrum. This noise, which has been called composite intermodulation noise (CIN), combines with thermal noise and determines the NTSC signal-to-noise (*S/N*) ratio. The NTSC *S/N* decreases with increasing digital signal level, thus placing an upper limit on the digital signal level relative to the analog signal. Nonlinearities in the system, including laser clipping, also cause the NTSC video signals to produce intermodulation noise which falls into both the NTSC spectrum and into the spectrum occupied by the digitally modulated signals. The magnitude of these intermodulation products can be reduced by using components which are more linear, by reducing the analog-signal levels relative to the digital-signal levels and by controlling the phase of the NTSC video carriers.

In general, the power in intermodulation distortion products at a given signal power level is determined by both the nonlinearities present in the transmission system and by the design of the composite signal waveform carried by the system. HFC systems with a top bandwidth of 750 MHz are frequently designed to transmit downstream NTSC video in the spectrum from 50 to 550 MHz and various downstream digitally modulated signals in the spectrum from 550 to 750 MHz. The spectrum from 5 to 40 MHz is often used to transmit signals from the home to the headend on the coaxial portions of the system. We discuss video-carrier phase-control techniques that minimize the NTSC intermodulation distortion which falls outside the spectrum occupied by the NTSC video signals, while also minimizing composite second-order (CSO) and composite triple-beat (CTB) distortion products. This results in an increase in the maximum capacity of the digital portion of the system and/or an improvement in the digital performance as well as an improvement in the NTSC performance. The system engineer also has an option, by using these techniques, of trading improved system performance for reduced system costs.

In this paper, the merits of phase control of the NTSC video carriers on the digital-signal performance will be stressed, along with the accompanying improvement in the NTSC performance. The BER performance of digital signals depends critically on both the peaking characteristic and the rms value of the intermodulation distortion products which fall into a channel occupied by digital signals. In a traditional CATV system in which the NTSC video-carrier frequencies are noncoherent, the peak/rms value of the broad-band waveform and both the peak/rms and rms value of the distortion products are statistical variables with large variances. This is due to slowly occurring changes in the frequencies and phases of the video carriers. The BER performance of the digital signals carried on these systems also slowly change or breath with time. The minimization of the peak/rms of the broad-band waveform by the control of the coherent NTSC video-carrier phase has the additional benefit of reducing laser clipping effects in an HFC system. Signal clipping is a gross nonlinear effect which produces broad-band distortions, thus, the high-order nonlinear effects (greater than third-order) in the system can be minimized via the minimization of the peak/rms quantity.

In Section II, the second- and third-order intermodulation products as functions of carrier phases are given. The minimization of the second-order distortion in the frequency-domain using the concept of an "ambiguity function" is discussed in Sections III and IV. In Section V, we apply the stationary-phase principle for a constant envelope FM signal to the minimization of the peak/rms ratio of the broad-band composite NTSC video-carrier waveform. For a flat-carrier spectrum, the optimal carrier phase relationship results in an extension of the well-known Newman phases. Generalization to the sloped-carrier spectrum using nonlinear FM is also discussed. In Section VI, we consider a general quadratic-phase relationship and use numerical techniques to study the relations between the second- and third-order distortion power, and the peak/rms of the broad-band waveform. A

Manuscript received March 31, 1997; revised August 15, 1997.

G. D. Alley is with the Lucent Technologies, Bell Laboratories, North Andover, MA 01845 USA.

Y. L. Kuo, retired, was with AT&T Bell Laboratories, North Andover, MA 01845 USA. He is now at Flat F, 10th Floor, Block 11, Royal Ascot, Shatin, N.T., Hong Kong.

Publisher Item Identifier S 0018-9480(97)08349-X.

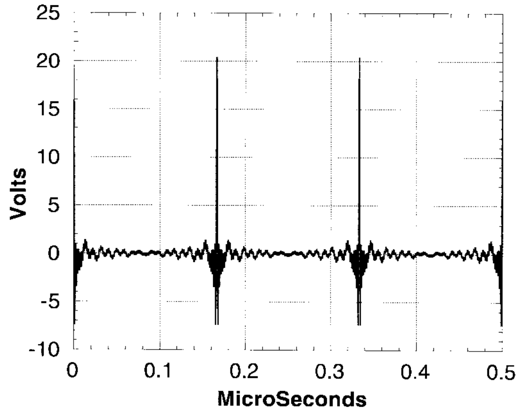

Fig. 1. Broad-band time-domain waveform. All 81 video-carrier phases are set to zero when $t = 0$.

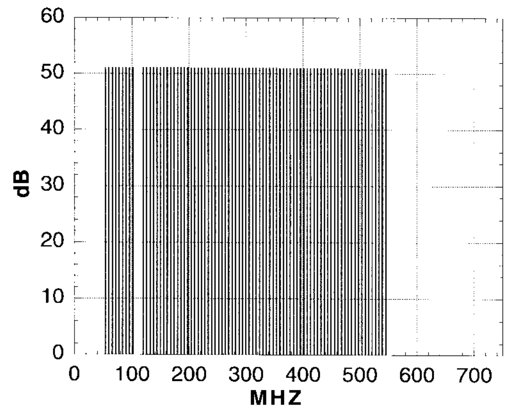

Fig. 2. Spectrum corresponding to the time-domain waveforms shown in Figs. 1 and 8.

25-channel system is used for the above illustration. The time-domain behavior of the out-of-band (digital band) third-order intermodulation distortions for a noncoherent system is also illustrated with numerical results for a 64-channel system. The slowly varying values of the peak intermodulation products which fall into the digital band are explained in this section. These variations in turn cause large variations in the BER of digital signals. Finally, an experimental coherent CATV system consisting of 81 live video channels and four 64 quadrature amplitude modulation (QAM) digital channels transported using a combination of linear lightwave and coaxial distribution systems is presented in Section VII. This demonstration system used commercially available equipment together with custom designed hardware, which controlled the video-carrier phases.

II. HFC Spectrum and Distortion Products

Consider the following signal as a model for the video carriers in an 83-channel (54–546 MHz) CATV system using the harmonically related carrier (HRC) frequency plan with $\omega_s = 2\pi 6 \times 10^6$:

$$v(t) = \sum_{n=9}^{91} a_n \cos(n\omega_s t + \phi_n). \tag{1}$$

It is customary with the HRC frequency plan not to use the two channels at 108 and 114 MHz ($n = 18$ and 19) in order to minimize interference into aircraft communication bands. If the carriers phases $\phi_n = 0$ when $t = 0$, for all n the waveform is given in Fig. 1 and the corresponding spectrum is given in Fig. 2. In these figures $a_{18} = a_{19} = 0$. The peak-to-rms ratio (peak/rms) of the broad-band signal in Fig. 1 is 22.1 dB.

The second- and third-order distortion products due to polynomial nonlinearities with unity coefficients (assumed for all calculations in this paper) are given by

$$\begin{aligned} v^2(t) = {} & \sum_{n=9}^{91} \frac{a_n^2}{2} + \sum_{n=9}^{91} \left(\frac{a_n^2}{2}\right) \cos(2n\omega_s t + 2\phi_n) \\ & + \sum_{\substack{n=9 \\ (n\neq m)}}^{91} \sum_{m=9}^{91} a_n a_m \cos[(n \pm m)\omega_s t + (\phi_n \pm \phi_m)] \end{aligned} \tag{2}$$

and

$$\begin{aligned} v^3(t) = {} & \frac{3}{4} \sum_{n=9}^{91} a_n^3 \cos(n\omega_s t + \phi_n) \\ & + \frac{1}{4} \sum_{n=9}^{91} a_n^3 \cos(3n\omega_s t + 3\phi_n) \\ & + \frac{3}{2} \sum_{\substack{n=9 \\ (n\neq m)}}^{91} \sum_{m=9}^{91} a_n a_m^2 \cos(n\omega_s t + \phi_n) \\ & + \frac{3}{4} \sum_{\substack{n=9 \\ (n\neq m)}}^{91} \sum_{m=9}^{91} a_n^2 a_m \\ & \cdot \cos[(2n \pm m)\omega_s t + (2\phi_n \pm \phi_m)] \\ & + \frac{3}{2} \sum_{\substack{n=9 \\ (n\neq m\neq k)}}^{91} \sum_{m=9}^{91} \sum_{k=9}^{91} a_n a_m a_k \\ & \cdot \cos[(n \pm m \pm k)\omega_s t + (\phi_n \pm \phi_m \pm \phi_k)]. \end{aligned} \tag{3}$$

From (2) and (3), we can see that some distortion product magnitudes are carrier phase-independent, but most distortion products (those in the double and triple summations) are carrier phase-dependent. In general, the distortion spectrum is maximized when all ϕ_n are equal at $t = 0$. Fig. 3 shows the second-order distortion spectrum and Fig. 4 the third-order distortion spectrum with $\phi_n = 0$ at $t = 0$ and $a_{18} = a_{19} = 0$.

We can see that large peak/rms values require excessive headroom in order to prevent the linear lightwave laser transmitter from clipping and that the distortion products extend both above and below the analog video spectrum. These distortions products can cause digital errors in both the upstream and downstream directions in HFC systems.

III. Control of Signal Distortion and Peaking

To minimize the distortion products over any frequency band, the relationship between the carrier phases can be set to the appropriate values and maintained at these values using appropriate phase-control techniques. However, the distortion minimization for a high capacity wide-band multicarrier system is a nontrivial problem. Several authors [1]–[3] have

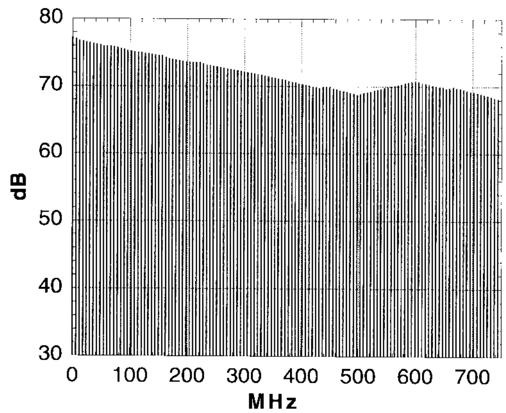

Fig. 3. Zero-phase (worst-case) second-order distortion spectrum with unity second-order coefficient.

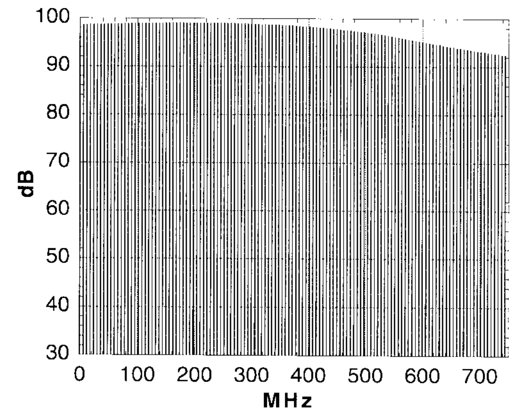

Fig. 4. Zero-phase (worst-case) third-order distortion spectrum with unity third-order coefficient.

worked on this problem with some success. In this paper, we will develop a general approach to the distortion minimization problem together with numerical simulation and experimental results.

Consider the composite multicarrier signal (1), which can be rewritten as (with $\Omega \equiv 8\omega_s$)

$$\begin{aligned} v(t) &= \mathrm{Re}\left[e^{j\Omega t}\sum_{k=1}^{83} a_k e^{j(k\omega_s t+\phi_k)}\right] \\ &= \cos(\Omega t)\left[\sum_{k=1}^{83} a_k \cos(k\omega_s t+\phi_k)\right] \\ &\quad - \sin(\Omega t)\left[\sum_{k=1}^{83} a_k \sin(k\omega_s t+\phi_k)\right] \end{aligned} \tag{4}$$

where Ω is considered as an arbitrarily assigned "center frequency" of the wide-band composite signal. The envelope of the above signal is defined as

$$E(t) = \sqrt{\begin{array}{l}\left[\sum_{k=1}^{83} a_k \cos(k\omega_s t+\phi_k)\right]^2 \\ + \left[\sum_{k=1}^{83} a_k \sin(k\omega_s t+\phi_k)\right]^2\end{array}}. \tag{5}$$

The squared envelope function is then given by

$$\begin{aligned} E^2(t) &= \sum_{k=1}^{83} a_k^2[\cos^2(k\omega_s t+\phi_k)+\sin^2(k\omega_s t+\phi_k)] \\ &\quad + \sum_{\substack{k=1\\(k\neq l)}}^{83}\sum_{l=1}^{83} 2a_k a_l[\cos(k\omega_s t+\phi_k)\cos(l\omega_s t+\phi_l) \\ &\qquad + \sin(k\omega_s t+\phi_k)\sin(l\omega_s t+\phi_l)] \\ &= \sum_{k=1}^{83} a_k^2 + 2\sum_{\substack{k=1\\(k\neq l)}}^{83}\sum_{l=1}^{83} a_k a_l \cos[(k-l)\omega_s t \\ &\qquad + (\phi_k-\phi_l)] \end{aligned} \tag{6}$$

which is periodic with a period $2\pi/\omega_s = \frac{1}{6}\ \mu\mathrm{s}$.[1]

[1] Note that the sum of frequency terms, $(k+l)\omega_s$, including the second harmonic components, all cancel out through trigonometric identities.

The $E^2(t)$ function contains no second harmonics of the carriers and no terms of the form $(k+m)\omega_s$. Comparing (6) and (2), it is interesting to note that $\frac{1}{2}E^2(t)$ is the same as the total second-order distortions at zero frequency and at all frequency components which are differences of carrier frequencies (i.e., $(k-l)\omega_s$ terms).

Borrowing from the classic pulse-compression radar-signal design theory [4], the $\frac{1}{2}E^2(t)$ is related to the "ambiguity function" for a discrete coded waveform (for the narrow-band case) as follows:

$$\Psi(\tau, \omega_d) = \sum_{k=1}^{N}\sum_{l=1}^{N}\int_{-\infty}^{\infty} u_k(t)u_l^*(t+\tau)e^{-j\omega_d t}\,dt \tag{7}$$

where

$$u_k(t) = a_k e^{j(k\omega_s t+\phi_k)} \tag{8}$$

is the "complex envelope" associated with each carrier at frequency $k\omega_s$. Using Parsevals' theorem, the ambiguity function can also be written as

$$\Psi(\tau, \omega_d) = \frac{1}{2\pi}\sum_{k=1}^{N}\sum_{l=1}^{N}\int_{-\infty}^{\infty} U_k^*(\omega)U_l(\omega+\omega_d)\cdot e^{-j\omega\tau}\,d\omega \tag{9}$$

where $U_k(\omega)$ is the Fourier transform of $u_k(t)$ and is given by

$$U_k(\omega) = 2\pi a_k e^{j\phi_k}\delta(\omega-k\omega_s). \tag{10}$$

Substituting (10) into (9) and after simplification, we have

$$\begin{aligned} &\Psi(\tau, \omega_d) \\ &\quad = 2\pi\sum_{k=1}^{N}\sum_{l=1}^{N} a_k a_l e^{[(\phi_k-\phi_l)-(k-l)\omega_s\tau]}\cdot\delta[\omega_d-(k-l)\omega_s]. \end{aligned} \tag{11}$$

With τ set equal to zero, (11) represents the $\frac{1}{2}E^2(t)$, as given in (6).

The ambiguity function [defined in (7) and (9)] as a two-dimensional (2-D) waveform amplitude-distribution function in time delay τ and frequency displacement ω_d has been the basis in modern radar technology for the systematic search for the best signal waveform for a particular application. Many results on the minimization of the side lobes relative to the dc value of the ambiguity function have appeared in the literature [4]. Even though these results are for narrow-band applications, they can be used to obtain various classes of candidate phases for the case of wide-band video carriers to achieve distortion minimization.

IV. Minimization of Envelope Variation

As seen in (6), the carrier phase-independent second-order distortion at dc is fixed when the carrier amplitudes a_k are given. To avoid the high peaks in the instantaneous $E^2(t)$ (a power quantity) and, consequently, high distortion at $(k-l)\omega_s$, we shall minimize the variation of $E^2(t)$ from its mean value of $\sum a_k^2$, which can be written as

$$\text{Variance}\left\{E^2(t) - \sum_{k=1}^{83} a_k^2\right\} = 2\sum_{k=1}^{83} |r_k|^2 \tag{12}$$

where

$$r_k \equiv \sum_{n=1}^{N-k} A_n A_{n+k}, \qquad k = 1, 2, \cdots, N = 83 \tag{13}$$

and $A_n \equiv a_n e^{j\phi_n}$, characterizing the nth carrier amplitude a_n and phase ϕ_n. The coefficient r_k can be interpreted as the autocorrelation values of the complex sequence $A_1, A_2, \cdots, A_N$. Minimizing (12) implies the total power in the sidelobes of the ambiguity function (for $\tau = 0$) is minimized. Many such codes (sequences) are available in the literature including maximal length pseudo random and Barker (for $N \leq 13$) binary codes, Frank, and other polyphase codes [4].

In a wide-band CATV application, the second-order distortion contains products of the type $(k+l)\omega_s$ as well as $(k-l)\omega_s$ terms and they generally overlap in frequency. Therefore, the approach of radar-signal design must be modified to treat the CATV problem. Fortunately, minimization of (12) also generally results in the reduction of the distortions at all other frequencies (including the overlap region). We have developed numerical techniques which extend the classic ambiguity function to the design of wide-band CATV signals with improved performance. Our strategy is to optimize the total second-order distortions given in (2) by obtaining the carrier phases so that the composite signal has a second-order distortion spectrum that is substantially a line spectrum at dc (the $\sum \frac{1}{2} a_k^2$ term) with the residual distortions at all other frequencies (including the overlaps) minimized. Recognizing that the third-order distortion spectrum is the convolution in the frequency-domain of the second-order distortion spectrum with the original composite signal spectrum itself, the third-order distortions in both the in-band (analog band) and out-of-band (digital band) frequencies will be generally minimized. In fact, with the second-order distortion behaving essentially like a line spectrum at dc having minimum side lobes, the third-order distortion will mainly contain the phase-independent cross-modulation distortion terms (in-band) with minimum out-of-band third-order distortion products.

V. Principle of Stationary Phase

In the previous section, we discussed the distortion optimization in the frequency domain via the minimization of the second-order distortion products in the squared envelope function and its extension to broad-band CATV applications. In the time domain, the peak amplitude of the analog video-signal waveform is related to the peak factor of its envelope function. Since the envelope $E(t)$ of a low peak/rms signal cannot fluctuate wildly, it follows that its envelope will usually give a low peak factor too [10]. The peak factor is defined as the maximum absolute value of the waveform divided by its rms value. Minimizing the peak/rms ratio in the signal waveform also reduces the distortion effects due to the nonlinearities in the CATV system (including the clipping of lasers). In this section, we will present a method for synthesizing a set of carrier phases that will generally minimize the peak/rms ratio of the signal.

In [5], Schroeder proposed a rule based on an application of the principle of stationary phase which enables the phases of a set of Fourier coefficients, whose magnitudes are specified, to be determined so that the peak factor of the corresponding waveform is low. He reasoned that a low peak factor would result if the waveform could be made to approximate an FM signal with constant envelope, because the FM signals have low peak factors. The success of this approximation becomes better as the number of sinusoidal Fourier components increases (corresponding to the high-index FM signals).

The problem is stated as follows. Given the magnitudes of the carriers (not necessarily equal), we shall approximate the periodic composite video signal (1) to a constant envelope FM signal

$$s(t) = A\cos[(\Omega t + \phi(t)] \tag{14}$$

whose complex envelope is given by

$$u(t) = Ae^{j\theta(t)} \tag{15}$$

where A is constant and $\theta(t)$ is periodic with period $T = 2\pi/\omega_s$. Then the Fourier-series coefficients in the expansion of (15) would approximate the prescribed power spectrum of the video carriers and the phases of the coefficients are to be chosen to minimize the peak factor of (1). We shall assume that $\theta(t)$ is a monotonic function of t such that for a given frequency $\omega = k\omega_s\,(k = 1, 2, \cdots, N = 83)$:

$$\theta'(t) - \omega = 0 \quad \text{(stationary phase)} \tag{16}$$

has a single solution at $t = t_k$ in the time interval (0, T) with $\theta''(t) = 0$ and no solution exists for $k > N$.

According to the principle of stationary phase [9, pp. 271–273] and [4, pp. 34–35], the Fourier-series coefficients of (15) for high-index FM (i.e., $N \gg 1$) are given by

$$u(t) = \sum_{k=-\infty}^{\infty} U_k e^{jk\omega_s t} \tag{17}$$

where

$$U_k = \frac{A}{T}\int_0^T e^{j[\theta(t)-k\omega_s t]}\,dt, \qquad k=1,2,\cdots \tag{18}$$

$$\approx \begin{cases} \dfrac{A}{T}\,e^{j[\theta(t_k)-k\omega_s t_k]}\sqrt{\dfrac{2\pi j}{\theta''(t_k)}}, & \text{for } k=1,\cdots,N \\ \text{“0” (Small)}, & \text{for } k>N \end{cases} \tag{19}$$

$$\approx \begin{cases} \dfrac{A}{T}\,e^{j(\phi_k \pm \pi/4)}\sqrt{\dfrac{2\pi}{|\theta''(t_k)|}}, & \text{for } k=1,\cdots,N \\ \text{“0” (Small)}, & \text{for } k>N \end{cases} \tag{20}$$

where

$$\phi_k \equiv \theta(t_k) - k\omega_s t_k = \theta_k - k\omega_s t_k \tag{21}$$

and the sign of $\pi/4$ is dependent on the sign of $\theta''(t_k)$ being positive or negative, respectively. The phase ϕ_k for the carrier frequency $k\omega_s (k=1,2,\cdots,N)$ will now be determined as a function of the prescribed carrier spectrum.

Case 1: For the flat-spectrum case, the magnitude of U_k is constant for $k=1,2,\cdots,N$, therefore, we set $\theta''(t_k) = 2b_2\,(b_2 \neq 0)$. Hence

$$\theta'(t) = 2b_2 t + b_1 \tag{22}$$

and

$$\theta(t) = b_2 t^2 + b_1 t + b_0 \tag{23}$$

which is a linear FM (chirp).[2] Substituting (22) into (16) and solving the stationary-phase equation at $t=t_k$, we obtain

$$t_k = \frac{(k\omega_s - b_1)}{2b_2} \tag{24}$$

and

$$\theta'(t_k) = k\omega_s, \qquad k=1,2=\cdots,N. \tag{25}$$

Assume $b_2 > 0$ and define

$$\Delta_k = t_k - t_{k-1} = \frac{\omega_s}{2b_2} \tag{26}$$

a constant independent of b_1. Dividing the period $T=2\pi/\omega_s$ by N segments of Δ_k, we obtain

$$b_2 = \frac{N\omega_s}{2T} = \frac{N\pi}{T^2}. \tag{27}$$

Hence, from (20), (21), and (24) we have (after simplification)

$$|U_k| \approx \frac{A}{\sqrt{N}}, \qquad \text{for } k=1,2,\cdots,N \tag{28}$$

and

$$\phi_k = \frac{(k\omega_s - b_1)^2}{4b_2} + b_0 = d_2k^2 + d_1k + d_0. \tag{29}$$

Note that from (29), the phase relationship of the flat-spectrum carriers is a quadratic equation in the frequency domain, as it should be from the time-domain quadratic characteristic of (23) (see Appendix A). If b_0 and b_1 are chosen to be zero, then $\phi_k = (\pi/N)k^2$, which is known to be the Newman phase relationship [6], [7]. In actual applications, optimal b_0 and b_1 for minimizing peak/rms of the signal can be obtained using numerical techniques. It is interesting to note that for the special case of $b_1 = \omega_s/2 = \pi/T$, ϕ_k becomes the results as prescribed by Schroeder [5].

[2] It is an upward chirp if $b_2 > 0$, and a downward chirp if $b_2 < 0$.

Case 2: For the linearly sloped spectrum $|U_k|^2 = a^{k-1}|U_1|^2$ for $k=1,\cdots,N$, a is assumed to be greater than 1 for an upwardly sloped spectrum. For this case, as well as for the general nonlinear FM case, we shall use the result in Appendix A to obtain the carrier phases that will minimize the peak-to-rms ratio of the signal. Thus, from (A10) we have

$$\begin{aligned}\tau_d(k\omega_s) &= -\phi'(k\omega_s)\\ &= -\int c_1 a^{(k-l)\omega_s}|U_1|^2\,d(k\omega_s) + c_2\\ &= -c_1'|U_1|^2\,\frac{a^{(k-l)}}{\ln(a)} + c_2.\end{aligned} \tag{30}$$

Imposing the boundary conditions

$$\tau_d(0) = 0 \text{ and } \tau_d(N\omega_s) = \frac{2\pi}{\omega_s} \tag{31}$$

we obtain

$$\tau_d(k\omega_s) = \frac{2\pi}{\omega_s}\,\frac{a^k}{a^N - 1} - \frac{2\pi}{\omega_s}\,\frac{1}{a^N-1}. \tag{32}$$

Integrating (32)

$$\begin{aligned}\phi_k &\equiv \phi(k\omega_s)\\ &= -\int \tau_d(k\omega_s)\,dk\omega_s + c_0\\ &= \frac{2\pi}{(a^N-1)\ln(a)}\,a^k - \frac{2\pi}{(a^N-1)}\,k + c_0 \qquad (33)\\ &= d_2(a)a^k + d_1(a)k + d_0 \qquad (34)\end{aligned}$$

where $d_2(a)$ and $d_1(a)$ are the nonlinear functions of a, as given in (33).

In general, for any spectral shape of $|U(\omega)|^2$, $\omega = k\omega_s$, $k=1,\cdots,N$, the carrier phases can be determined by the above procedure. This includes the missing channels over the CATV bands.

VI. Numerical Results

From (29), if we fix d_2 and vary d_1 or d_0, we see interesting relationships between the peak/rms of the broadband waveform, the second-order distortion power (P_2), and the third-order distortion power (P_3). P_2 is defined as the total second-order distortion power over any band of interest. P_3 is defined as the total out-of-band third-order distortion power over the band of interest. The in-band third-order distortion power is excluded from P_3 since it contains terms which are phase independent (cross modulation terms). With optimal phases these cross modulation terms become the dominant in-band third-order distortion power, but do not contribute to the out-of-band distortion.

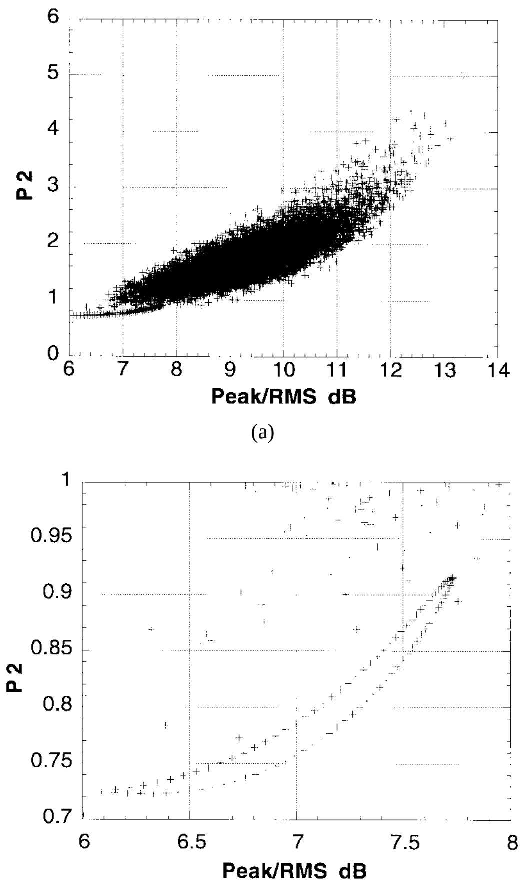

Fig. 5. Contours in the P/rms (dB) p_2 plane produced by varying d_1 over a range of $2\pi/16$ for fixed values of D_0 and d_2 together with the results of 10 000 sets of video phases uniform over $0 \leq \phi_n \leq 2\pi$.

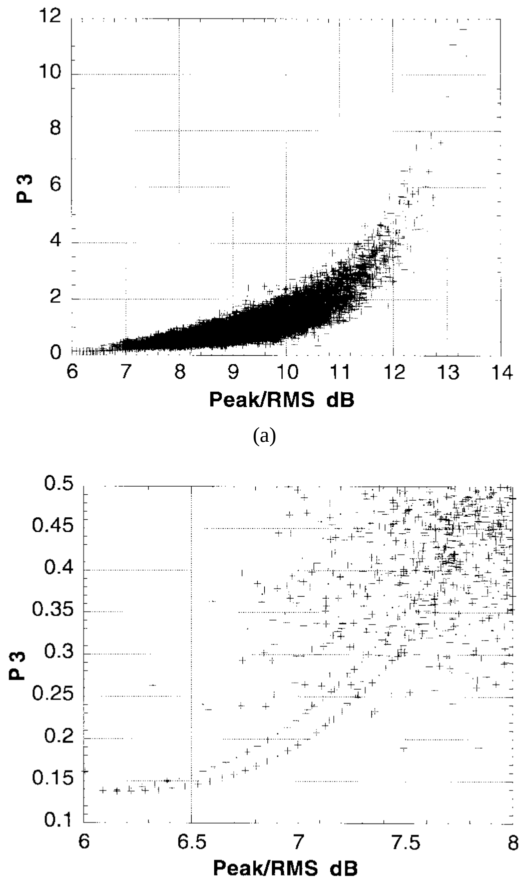

Fig. 6. Contours in the P/rms (dB) p_3 plane produced by varying d_1 over a range of $2\pi/16$ for fixed values of D_0 and d_2 together with the results of 10 000 sets of video phases uniform over $0 \leq \phi_n \leq 2\pi$.

Using a 25-channel system as an example, with the two channels at 114 and 120 MHz missing, the relationships between P_2 and peak/rms [Fig. 5(a) and (b)], P_3 and peak/rms [Fig. 6(a) and (b)], and P_2 and P_3 [Fig. 7(a) and (b)] are shown for two sets of data. The first set contains the results of 10 000 groups of uniformly distributed video-carrier phases $0 \leq \phi_n \leq 2\pi$, and in the second set d_1 is varied over a range of $2\pi/16$ with fixed values for d_0 and d_2. Figs. 5(b), 6(b), and 7(b) are expanded views which show the closed contours produced by the variation in d_1 along with the drastic improvements in P_2, P_3, and peak/rms relative to the random video-carrier phase cases. Note that in Fig. 7(b), the relationship between P_2 and P_3 appears to be elliptical. An explanation of this behavior is given in Appendix B. Data similar to that shown in Figs. 5–7 allow us to pick values of d_2, d_1, and d_0 for a given set a_n which optimize P_2, P_3, and peak/rms over any defined frequency bands using any desired weighting function.

For the 83 channel spectrum, with the two channels at 114 and 120 MHz missing, (shown in Fig. 2) values of ϕ_k, calculated using values of d_2, d_1, and d_0 in (29), which minimize the peak/rms of the broad-band waveform have been selected. The voltage waveform in this case is shown in Fig. 8 along with the corresponding distortion spectrums in Fig. 9 (second order) and Fig. 10 (third order). The peak/rms value of the broad-band waveform has been reduced from 22.1 dB (Fig. 1) to 5.5 dB and the second- and third-order distortions have been improved by more than 15 and 30 dB, respectively, from the worst case (Figs. 3 and 4) over the entire band.

Figs. 11 (flat spectrum) and 12 (7-dB upward slope from 50 to 550 MHz) show the range of third-order distortion products when the carrier phases ϕ_n are varied from zero to phases which minimize P_3. The three center curves in Figs. 11 and 12 show the 99.8% upper and lower bounds on the rms value of P_3 as ϕ_n are selected from a uniform distribution over $0 \leq \phi_n \leq 2\pi$. We see that the in-band rms values of the third-order distortion vary by over 3 dB while the out-of-band rms values of the third-order distortion vary by over 4 dB. The zero-phase case increases third-order distortion by about 30 dB relative to the mean random phase value while the optimum phases reduce the out-of-band rms values of the third-order distortion by approximately 16 dB relative to the mean random-phase value.

When using the standard-frequency plan common-system design practice results in rms values of the second- and third-order distortion products CSO and CTB, which are approximately equal. Under these conditions, the most important distortion product which falls into the digital band is the third-

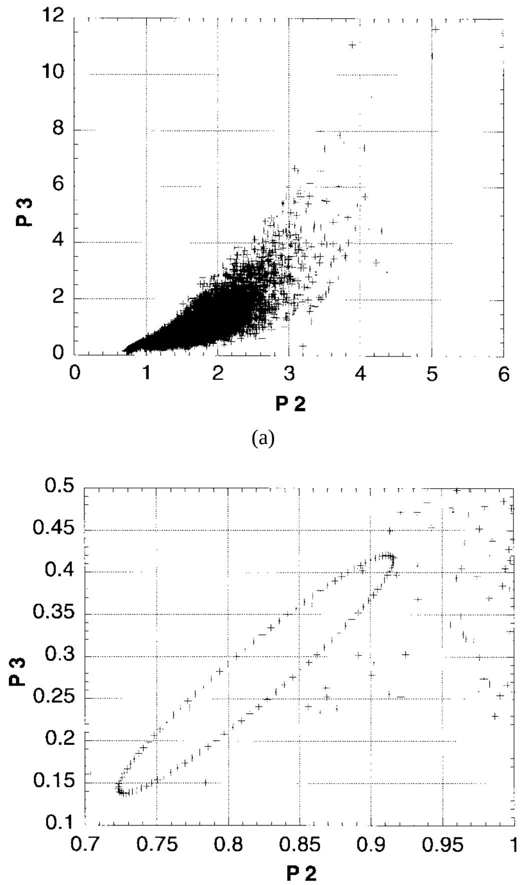

(a)

(b)

Fig. 7. Contours in the P_3–P_2 plane produced by varying d_1 over a range of $\frac{2\pi}{16}$ for fixed values of D_0 and d_2 together with the results of 10 000 sets of video phases uniform over $0 \leq \phi_n \leq 2\pi$.

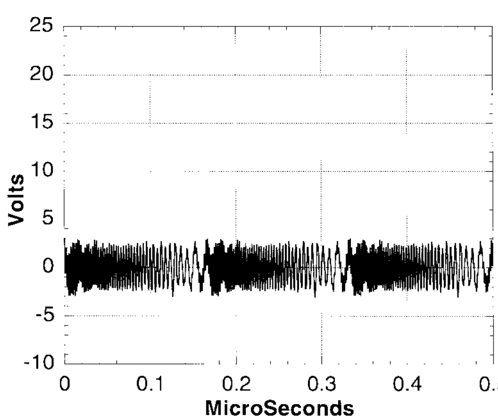

Fig. 8. Broad-band time-domain waveform. All 81 video-carrier phases are set to values which minimize the third-order distortion products due to the video carriers which fall into the digital band.

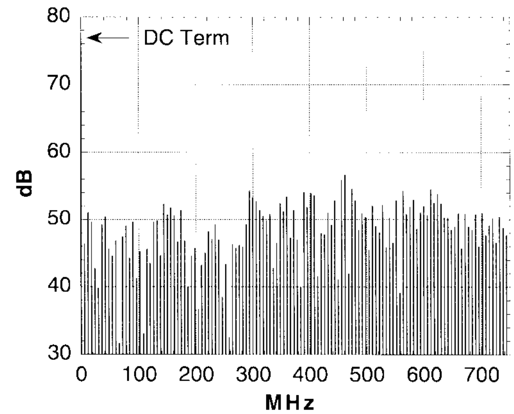

Fig. 9. Second-order distortion spectrum with unity second-order coefficient, calculated under the conditions of Fig. 8.

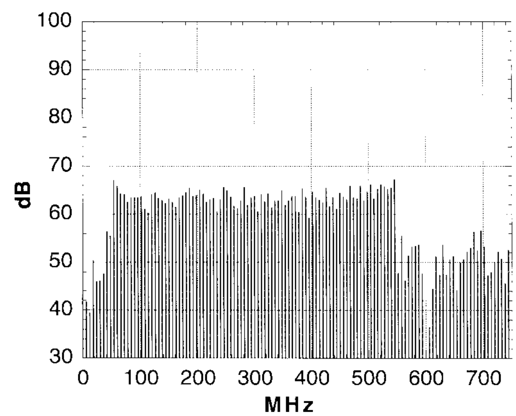

Fig. 10. Third-order distortion spectrum with unity third-order coefficient, calculated under the conditions of Fig. 8.

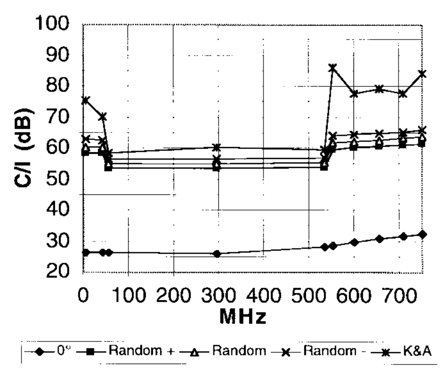

Fig. 11. Third-order carrier to distortion results for optimal peak/rms K&A phases, zero phase (worst case), random phases showing 0.1% and 99.9% limits, and 81-channel flat-analog spectrum.

order due to the high peak/rms value of third-order products relative to the peak/rms value of second-order products. (This should not be confused with the peak/rms values of the broad-band video signal $v(t)$, which is shown in Fig. 1). The digital signal will make errors when the interfering voltage produced by intermodulation products, which fall into the digital channel, cause the received signal to cross a decision threshold. For this reason, it is desirable to optimize the analog signal such that the third-order products which fall into the digital band have both a minimum rms value and a minimum peak/rms value.

In order to study the time domain behavior of the out-of-band third-order intermodulation products, we have used the closed-form expressions for all of the third-order distortion products (3), produced by a 64-channel system ($9 \leq n \leq 72$ with all $a_n = 1$). At 708 MHz, there are 575 products of the form $n \pm m \pm k$ and 41 products of the form $2n \pm m$.

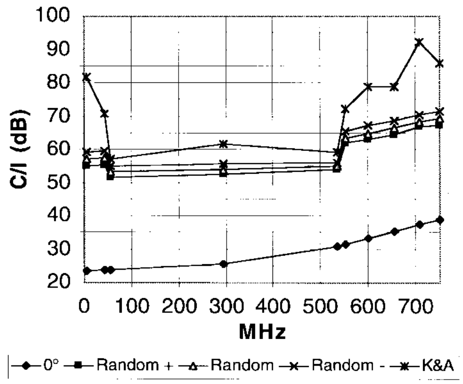

Fig. 12. Third-order carrier to distortion results for optimal peak/rms phase, zero phase (worst case), random phases showing 0.1% and 99.9% limits, and 81-channel analog spectrum with 7-dB up slope from 50 to 550 MHz.

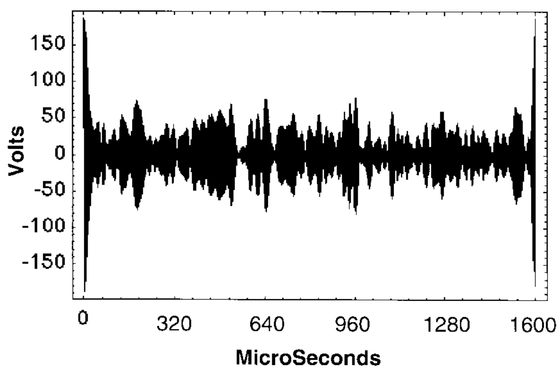

Fig. 13. Time-domain waveform for third-order distortion product which falls at 702 MHz with random phases and random frequency offsets from nominal. Since the frequency offsets are randomly selected from steps of 635 MHz, the waveform is periodic with a period of 1.6 ms.

The carrier frequencies have been assigned quantized random offsets from their nominal value as shown in (35):

$$v(t) = \sum_{n=9}^{72} a_n \cos\left[(n\omega_s + 2\pi\Delta f_n)t + \phi_n\right]$$
$$-15\,625 \le \Delta f_n \le 15\,625$$
$$\text{with a step size of } 625 \text{ Hz.} \tag{35}$$

The time behavior of $v(t)$ and the distortion products are then periodic with a period of 1.6 ms, which is the reciprocal of the greatest common divisor (625 Hz) of the frequency offsets. In the numerical simulations, we then look at each set $(\phi_n, \Delta f_n)$ over one period of the waveform in order to calculate the statistics of the process.

Figs. 13 and 14 show the time-domain behavior of third-order products falling into the digital channels at 702 and 708 MHz for one set of random phases ϕ_n, and random frequency offsets Δf_n. For this particular case, the peak/rms value of the third-order products are 15.9 and 16.2 dB at 702 and 708 MHz, respectively. If $\phi_n = 0$, the peak/rms value of these products increase to over 29 dB. As the phases ϕ_n approach unfavorable sets, both the rms values of the third-order products and the peak/rms values of these products rapidly increase. In Fig. 15(a) ($\phi_n = 0$) and (b) ($0 \le \phi_n \le 2\pi$), we see that the duration of the peaks in the third-order products is on the order of the reciprocal of the frequency spread around the nominal frequencies. In this case, the width—6 dB below the peak—is approximately $1/(3 \times 15\,625) = 21$ μs. If the bit rate for a 64 QAM digital signal is 30 Mb/s, then this would result in an error burst which lasted for about 640 b. An error burst of this length would be difficult to correct using standard error-correction techniques.

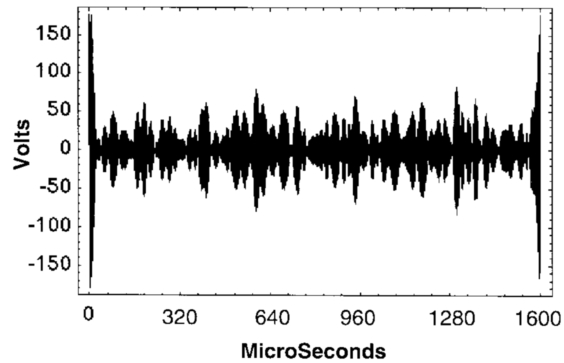

Fig. 14. Time-domain waveform for third-order distortion product which falls at 708 MHz with random phases and random frequency offsets from nominal. Data calculated as in Fig. 13.

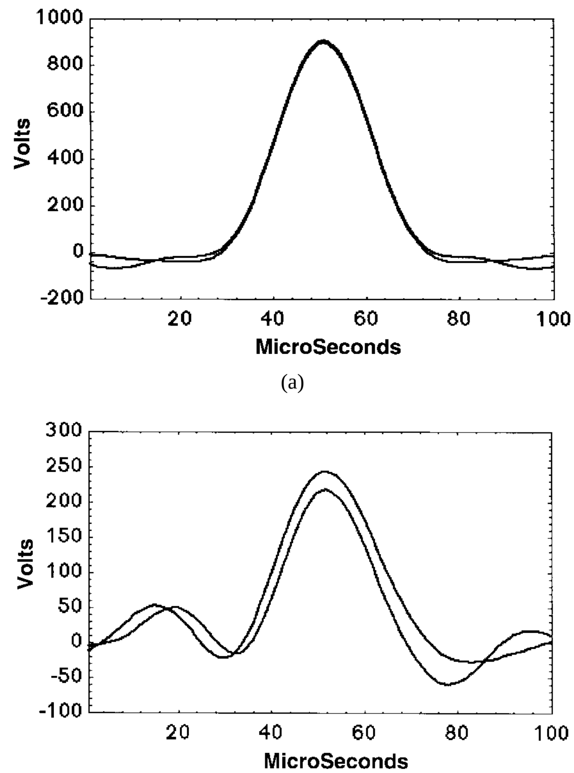

Fig. 15. (a) Time-domain waveform for third-order distortion products which falls at 702 and 708 MHz with zero carrier phases. (b) Time-domain waveform for third-order distortion products which falls at 702 and 708 MHz with one set of random-carrier phases.

In the HRC frequency plan, the errors from the nominal 6-MHz channel spacing are zero and the intermodulation products due to video carriers become tones with a peak/rms of 3 dB. For the incrementally related carriers (IRC's) frequency

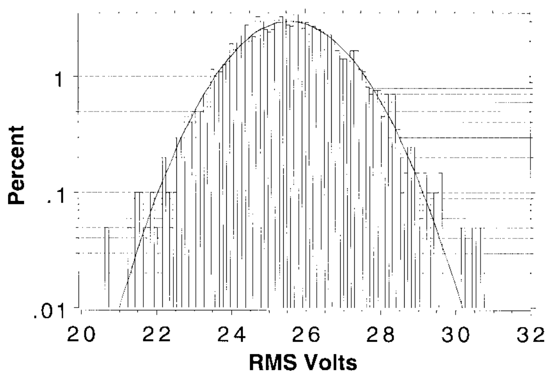

Fig. 16. Distribution of rms voltages of one third-order product which falls at 708 MHz. Data calculated using random-carrier phases and frequency offsets.

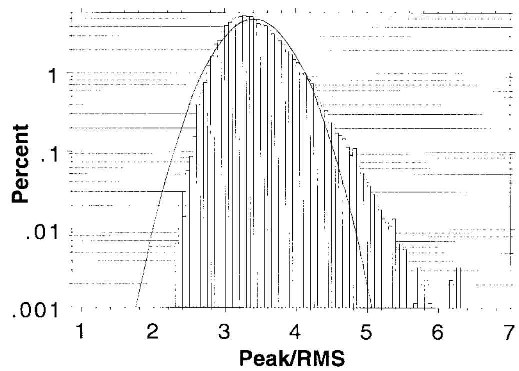

Fig. 17. Distribution of peak/rms voltages of one third-order product which falls at 708 MHz. Data calculated using random-carrier phases and frequency offsets.

plan, the peak/rms ratio of the distortion products exceeds that of the HRC plan and is thus less desirable.

Under the conditions given in (31), using closed-form equations for the third-order distortion products which fall at 702 and 708 MHz in a 64-channel system, we have calculated the statistics of the rms value of the third-order products as well as the statistics of the peak/rms value of the third-order products. As seen in Fig. 16, the rms values of the distortion in any out-of-band channel follow a normal distribution if ϕ_n is randomly distributed $0 \le \phi_n \le 2\pi$. In addition to the variation in the rms values of the third-order distortion, the peak/rms values of a single product change as the carrier phases are selected from a $0 \le \phi_n \le 2\pi$ uniform distribution. Fig. 17 shows the probability density function (PDF) for the peak/rms of a single third-order product which falls at 708 MHz. In this case, the PDF is not normal, but rather appears to be Maxwellian. The maximum value of the peak/rms exceeds the mean value of the peak/rms by 9 dB with a probability of 10^{-5}.

In the standard frequency plan, as well as conventional implementations of the IRC and HRC frequency plans, the video-carrier phases are uncontrolled and drift with time. As the phases drift into ranges which produce high rms values and high peak/rms values for the third-order distortion products, the digital performance of the system will degrade. As discussed above, the duration of the peaks in the third-order distortion products are on the order of the reciprocal of three times the frequency spread around the nominal frequencies in each frequency plan. For example, in the standard plan, if all channels are within 1 kHz of the nominal frequencies, then the peaks in the third-order distortion products will last on the order of 1/3 ms. A 64 QAM modem with a bit rate of 30 Mb/s could thus have error bursts containing on the order of 10 000 b. As the carrier phases and frequency offsets slowly drift, the peaks of the intermodulation products will breath. This results in a digital BER floor, which is a slowly changing function of time. This breathing problem has been observed in field tests [11] as well as in our laboratory experiments.

VII. Experimental Results

We have constructed an 83-channel HRC headend. This headend contained 81 Scientific Atlanta 6350 video modulators using the HRC frequency plan and 81 Standard Telecom integrated receiver descrambler (IRD) satellite receivers. The satellite receivers supply independent live video signals to the baseband inputs of the video modulators. As in the simulations above, the channels at 108 and 114 MHz were unused, leaving 81 active video channels. The phases of the 81 video carriers were controlled in real time using specially constructed equipment to replace the Scientific Atlanta comb generator which normally supply the RF reference frequencies to the phase lock inputs of the video modulators. By changing the phase of the reference to the appropriate values, we could cause the phase of the video carriers to be equal to the desired set ϕ_n at the output of the headend RF combiner network. The phase feedback loop, which was an integral part of the phase control equipment, ensured that the desired phases were stable with time. During the experimental tests, various digital signals were also combined with the analog NTSC spectrum using the passive combining network at the headend output.

The output of the headend was connected to a distribution system consisting of an AT&T linear lightwave transmitter, 10 km of fiber, and an AT&T linear lightwave receiver. The output of the lightwave receiver then feeds a cascade of three General Instrument coaxial CATV amplifiers separated by appropriate lengths of coaxial cable. The third amplifier in this cascade was in turn connected to a tap which allowed us to monitor the signals on the system at the end of the transmission system.

While operating this system at standard operating levels, by varying the phase of the video carriers, we have been able to vary the intermodulation products which fall into the digital band from an equivalent rms carrier-to-interference level (C/I) of less than 0 dB to a C/I of greater than 50 dB. Using standard National Cable Television Association (NCTA)[3] measurements, the mean values of the combined CTB and CSO, which both fall at multiples of ω_s in the HRC frequency plan, were greater than 52 dB when the carrier phases were randomly selected $0 \le \phi_n \le 2\pi$. This demonstrates that the equipment was operated under conditions representative of good engineering practice.

[3] National Cable Television Association, *NCTA Recommended Practices for Measurements on Cable Television Systems,* 2nd ed., Oct. 1993.

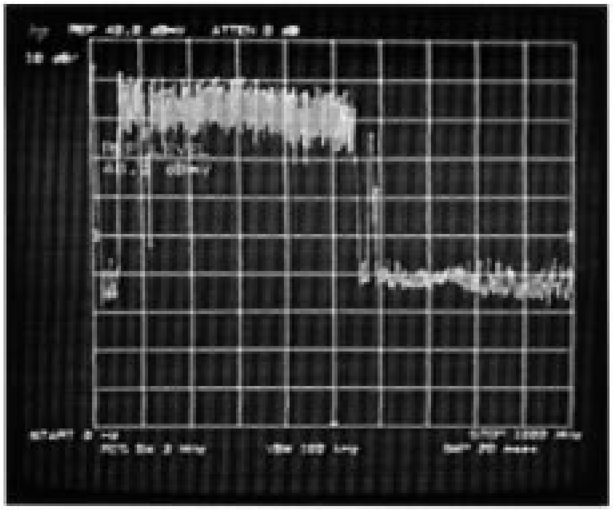

Fig. 18. Broad-band spectrum of the coaxial transmission system measured at the end of line tap following the three General Instruments 750-MHz coaxial amplifiers. Input spectrum to the first amplifier consists of 81 channels of live NTSC video together with a 64 QAM 30-Mb/s signal at 583 MHz with a level 10 dB below the analog level. Optimal peak/rms phases.

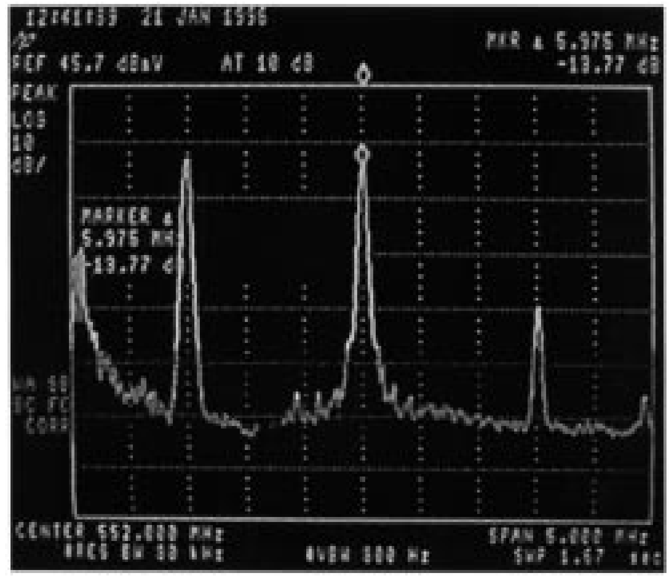

Fig. 19. A 5-MHz-wide spectrum centered at 552 MHz, as in Fig. 18. Zero phase (worst case). This is adjacent to the last NTSC channel (video carrier at 546 MHz). The audio carrier of the highest NTSC channel, which is carrying live audio, falls at 550.5 MHz. This audio carrier is 15 dB below the peak of the 546-MHz video-carrier sync tip and is 1.5 MHz below the intermodulation distortion product which falls at 552 MHz (HRC frequency plan). The spectrum of the live video is shown on the left side of the figure. The intermodulation power is shown to be 14.5 dB at 552 MHz.

Using this equipment we were able to measure the digital performance of 64 QAM modems over long time periods with various power levels relative to the analog signals and various sets of ϕ_n for the analog signals. In addition, MPEG video signals were carried using commercial 64 QAM frequency translation equipment and 64 QAM modems. Long-term digital BER measurements, for various phase conditions and digital-channel frequencies were made on the system using 64 QAM cable modems driven by BER test sets and compressed digital video signals. The results of these measurements demonstrated the importance of video-carrier phase control to digital-signal performance in HFC systems.

The composite wide-band signal consisting of 81 video channels carrying independent live programming together with four digital signals could be set to provide peak/rms values which ranged from 22 to 5.5 dB. The technique used to set the video-carrier phases produced a stable system. For example, with the carrier phases set to produce a peak/rms value of 5.5 dB, the system was designed to maintain these conditions indefinitely.

Fig. 18 shows the broad-band spectrum of the coaxial transmission system measured at the end of line tap following the three General Instruments 750-MHz coaxial amplifiers. In this measurement, the linear lightwave transmitter and receiver were not used in the distribution system, thus removing the laser clipping nonlinearities from the results. The amplifiers have been adjusted with 10 dB of up slope from 50 to 750 MHz. The input spectrum to the first amplifier consists of 81 channels of live NTSC video together with a 64-QAM 30-Mb/s signal at 583 MHz with a level 10 dB below the analog level. The values of ϕ_n have been set to minimize the peak/rms value of the broad-band waveform.

Fig. 19 shows a 5-MHz wide spectrum centered at 552 MHz, measured under the same conditions as Fig. 18 with the exception that the values of ϕ_n have been set to zero to maximize the peak/rms value of the broad-band waveform. The portion of the spectrum shown in Fig. 19 is adjacent to the last NTSC channel (video carrier at 546 MHz). The audio carrier of the highest NTSC channel, which is carrying live audio, falls at 550.5 MHz. This audio carrier is 15 dB below the peak of the 546-MHz video-carrier sync tip and is 1.5 MHz below the intermodulation distortion product which falls at 552 MHz (HRC frequency plan). The spectrum of the live video is shown on the left side of the figure. The C/I (second-order + third-order) is shown to be 14.54 dB at 552 MHz. When the linear lightwave transmitter and receiver was included in the system for this measurement, laser clipping caused the C/I for the 64-QAM digital signal was less than 0 dB.

Fig. 20 shows a 5-MHz-wide spectrum centered at 552 MHz taken under the same conditions as in Fig. 19, except that the values of ϕ_n have been set to minimize the peak/rms value of the broad-band waveform. As in Fig. 19, the spectrum of the live video is shown on the left side of the figure. The C/I (second-order + third-order) is shown to be 56.72 dB at 552 MHz. The improvement over the results shown in Fig. 18 is over 42 dB.

Fig. 21 shows the broad-band spectrum from 550 to 750 MHz taken under the same conditions as Fig. 19 where the values of ϕ_n have been set to zero to maximize the peak/rms value of the broad-band waveform.

Fig. 22 shows the broad-band spectrum from 550 to 750 MHz taken under the same conditions as Fig. 20 where the values of ϕ_n have been set to minimize the peak/rms value of the broad-band waveform. The improvement over Fig. 21 ranges between 30 and 40 dB. Since we were not using 6-MHz-wide bandpass filters with RF preamplifiers to reduce the noise figure of the spectrum analyzer in this measurement, the dynamic range of this measurement, and

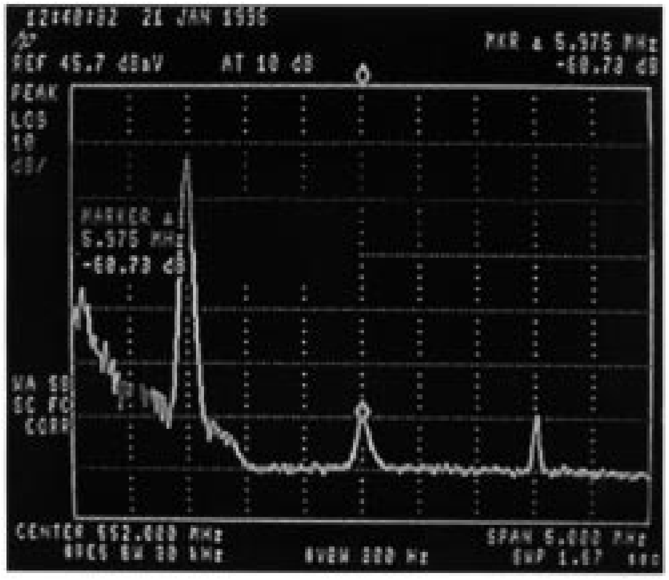

Fig. 20. As in Fig. 19, with optimal peak/rms phases. The intermodulation power is shown to be 56.7 dB at 552 MHz. The improvement of the results of Fig. 16 is over 42 dB.

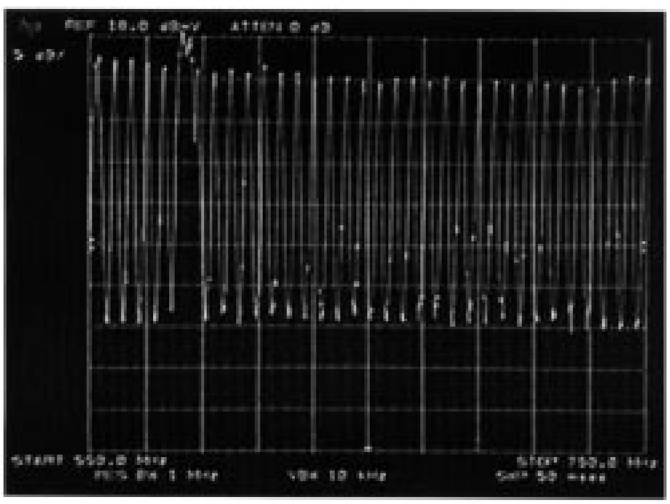

Fig. 21. Broad-band spectrum from 550 MHz to 750 MHz. Amplifiers have been adjusted with 10 dB of up slope from 50 to 750 MHz. Zero phase (worst case) as in Fig. 19.

thus the improvement in measured C/I, is limited by the spectrum analyzer noise.

VIII. Conclusions

We have presented a general approach (both in the frequency and time domains) to the distortion optimization in a phase-controlled HFC CATV system. The classic concepts of ambiguity function and the principle of stationary phase have been applied to the control of video-carrier phases for minimizing the intermodulation distortions in the digital bands. Based on the theoretical analysis, numerical techniques have been developed to minimize the peak/rms ratio of the broadband signal and the second- and third-order intermodulation products and applied to an 81-channel HRC headend. Drastic distortion improvement of the phase-controlled headend over the standard noncoherent headend has been demonstrated. An experimental coherent CATV system consisting of 81 live video channels and four 64 QAM digital channels has been set up. The measurement results confirm the analysis and prove that the phase-controlled HRC headend is a viable method for both performance improvement and cost reduction in HFC CATV systems.

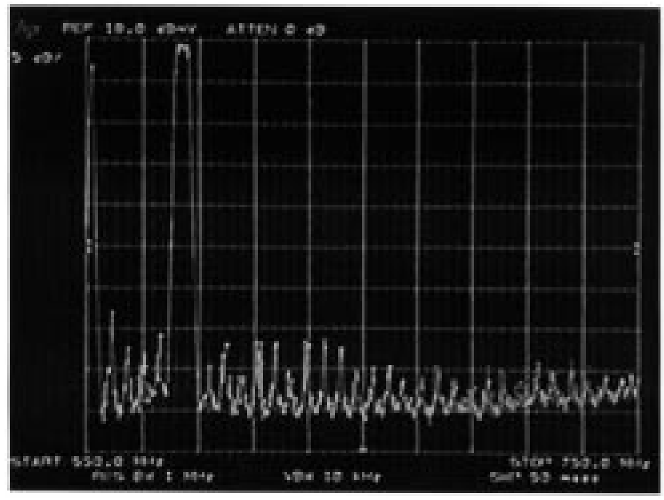

Fig. 22. Same conditions as Fig. 21 except that optimal peak/rms phases are used. The improvement over Fig. 21 ranges between 30–40 dB. Since we were not using 6-MHz-wide bandpass filters with RF preamplifiers in this measurement, the dynamic range of this measurement is limited by the spectrum-analyzer noise.

Appendix A

We could have obtained the result of (29) by the following argument based on the method of stationary phase for the analog continuous case as discussed in [4]. Following [4, pp. 41–42], the stationary-phase conditions are prescribed by

$$\theta'(t) = \omega \text{ and } \phi'(\omega) = -t. \tag{A1}$$

Let $\theta'(t) = \omega(t)$ and $\phi'(\omega) = -\tau_d(\omega)$, then (A1) becomes

$$\omega = \omega(t) \quad t = \tau_d(\omega). \tag{A2}$$

From the above, we obtain

$$\omega(t) = \tau_d^{-1}(t). \tag{A3}$$

Equation (A3) shows that the instantaneous frequency function $\omega(t)$ and the group-delay function $\tau_d(\omega)$ are inverse functions of each other. This important property of the principle of stationary phase will become the basis for the system's equalizer design (to be subsequently discussed).

For the flat-spectrum case, as shown in (22)

$$\theta'(t) = 2b_2 t + b_1, \qquad t \in (0, T)$$

we obtain

$$t = \frac{(\omega - b_1)}{2b_2}. \tag{A4}$$

Applying (A1), we have

$$\phi'(\omega) = -\tau_d(\omega) = -\frac{(\omega - b_1)}{2b_2}. \tag{A5}$$

Hence

$$\phi(\omega) = -\frac{(\omega - b_1)^2}{4b_2} + b_0. \tag{A6}$$

Replacing the continuous ω by the discrete frequency components $k\omega_s$, $k = 1, \cdots, N$, we have

$$\phi_k \equiv \phi(k\omega_s) = -\frac{(k\omega_s - b_1)^2}{4b_2} + b_0$$

which is the same as (29).

Following the development discussed in [4], the relation between the envelope $|u(t)|$ of (15) and the magnitude of its Fourier transform $U(\omega) \equiv |U(\omega)|e^{j\phi(\omega)}$ is given as

$$|\phi''(\omega)| \approx \frac{1}{2\pi}\,\frac{|U(\omega)|^2}{|u(t)|^2}, \qquad \text{for } \omega = \omega_k \tag{A7}$$

or its dual relation

$$|\theta''(t)| \approx 2\pi\,\frac{|u(t)|^2}{|U(\omega)|^2}, \qquad \text{for } t = \tau_d. \tag{A8}$$

For constant envelope FM signals having minimum peak-to-rms ratio, we obtain from (A7)

$$\frac{d\tau_d(\omega)}{d\omega} \equiv -|\phi''(\omega)| \approx -c_1|U(\omega)|^2. \tag{A9}$$

Hence

$$\tau_d(\omega) \approx \int c_1|U(\omega)|^2\, d\omega + c_2. \tag{A10}$$

Equation (A10) is the basis for the determination of the carrier phases for a general spectral shape. It is also the basis for the equalizer design when the transmitted signal undergoes linear distortion in the system.

Appendix B

We shall show that the parametric plot of the second-order distortion power of any frequency band versus the third-order distortion power of any other frequency band as a function of d_0 and d_1 is a closed curve, which is generally an ellipse. First consider the second-order distortion voltage in (2). The second-order distortion product at the frequency $(n \pm m)\omega_s$ is of the form

$$A_{nm} \cos[(n \pm m)\omega_s t + (\phi_n \pm \phi_m)] \tag{B1}$$

where $A_{nm} = \beta a_n a_m$, and $\beta = \frac{1}{2}$ for $n \neq m$ and $\beta = \frac{1}{2}$ for $n = m$. We calculate the power of the second-order distortion over any frequency band by squaring the sum of all (B1) terms over the band of interest

$$v_2^2(t) = \left\{ \sum_{n,m} A_{nm} \cos[(n \pm m)\omega_s t + (\phi_n \pm \phi_m)] \right\}^2. \tag{B2}$$

For example, the frequency components of interest are specified at $\omega = K\omega_s$, $K = K_1, K_2, \cdots, K_M$. That is, in (B2) we include all terms such that $n \pm m = K_1$, $n \pm m = K_2, \cdots$, and $n \pm m = K_M$ (with $n, m = 1, 2, \cdots, N$). Expanding (B2), each term is of the form $\cos(A)\cos(B)$, which is equal to $\frac{1}{2}\cos(A+B) + \frac{1}{2}\cos(A-B)$. Since the power of the second-order distortion is the integral of $v_2^2(t)$ over a period $= 2\pi/\omega_s$, we can discard all of the $\frac{1}{2}\cos(A+B)$ terms and we can discard the terms in $\frac{1}{2}\cos(A-B)$ that involve A and B from different $K\omega_s$ frequency components in the power calculation because they are harmonics of ω_s. Therefore, the second-order distortion power becomes

$$\begin{aligned}
P_2 &= \frac{1}{2}\left\{ \sum_{n\pm m=K_1} A_{nm}^2 + \sum_{n\pm m=K_2} A_{nm}^2 \cdots + \sum_{n\pm m=K_M} A_{nm}^2 \right\} \\
&\quad + \sum_{\substack{i \\ (i\neq j)}} \sum_j A_{K_1,i} A_{K_1,j} \\
&\quad \cdot \cos[\phi_{n\pm m=K_1,i} - \phi_{n\pm m=K_1,j}] \\
&\quad + \sum_{\substack{i \\ (i\neq j)}} \sum_j A_{K_2,i} A_{K_2,j} \\
&\quad \cdot \cos[\phi_{n\pm m=K_2,i} - \phi_{n\pm m=K_2,j}] \\
&\quad + \cdots + \sum_{\substack{i \\ (i\neq j)}} \sum_j A_{K_M,i} A_{K_M,j} \\
&\quad \cdot \cos[\phi_{n\pm m=K_M,i} - \phi_{n\pm m=K_M,j}]
\end{aligned} \tag{B3}$$

where the terms following the first bracketed term are due to the cross-product terms in (B2) that are of the same frequency with $n \pm m = K$, but of distinct set of (n, m); $A_{K,i} \equiv A_{n,m}$ with $n \pm m = K$ and i denotes the distinct set of (n, m); and $\phi_{n\pm m=K,i} \equiv \phi_n \pm \phi_m$ with $n \pm m = K$ and the corresponding ith distinct (n, m) set.

We now apply the above analysis to the CATV's HRC frequency plan with frequencies starting at 54 MHz. Using the quadratic-phase relationship of (29) for the flat-spectrum case, at the nth harmonic of $\omega_s = 6$ MHz

$$\phi_n = d_0 + (n-8)\,d_1 + (n-8)^2\,d_2 \tag{B4}$$

where $n = 9, 10, \cdots, (N+8)$ for an N-channel system.

Hence

$$\begin{aligned}
\phi_n \pm \phi_m &= (d_0 \pm d_0) + [(n-8) \pm (m-8)]\,d_1 \\
&\quad + [(n-8)^2 \pm (m-8)^2]\,d_2 \\
&= \begin{Bmatrix} 2 \\ 0 \end{Bmatrix} d_0 + \begin{Bmatrix} (n+m) - 16 \\ (n-m) \end{Bmatrix} d_1 \\
&\quad + \begin{Bmatrix} (n-8)^2 + (m-8)^2 \\ (n-8)^2 - (m-8)^2 \end{Bmatrix} d_2.
\end{aligned} \tag{B5}$$

Generally, d_2 is constrained by the number of channels in the system, and is typically approximately equal to π/N. Therefore, for a fixed d_2, a typical cosine term inside the second bracket of (B3) will be either of the form

$$\cos[2d_0 - 16\,d_1 + d_2 \cdot \text{function of } (n, m)] \tag{B6a}$$

or

$$\cos[d_2 \cdot \text{function of } (n, m)] \tag{B6b}$$

which is periodic in d_0 and d_1 with periods equal to π and $2\pi/16$, respectively. Since all the cosine terms in (B3) are periodic with respect to d_0 and d_1, we can combine all of the cosine terms which have the same period in (B3) to become a

$$\begin{aligned}\phi_n \pm \phi_m \pm \phi_k &= (d_0 \pm d_0 \pm d_0) + [(n-8) \pm (m-8) \pm (k-8)]\, d_1 + [(n-8)^2 \pm (m-8)^2 \pm (k-8)^2]\, d_2 \\ &= \left\{\begin{matrix} 3 \\ 1 \\ -1 \end{matrix}\right\} d_0 + \left\{\begin{matrix} (n+m+k)-24 \\ (n+m-k)-8 \text{ or } (n-m+k)-8 \\ (n-m-k)+8 \end{matrix}\right\} d_1 \\ &\quad + \left\{\begin{matrix} (n-8)^2 + (m-8)^2 + (k-8)^2 \\ (n-8)^2 + (m-8)^2 - (k-8)^2 \text{ or } (n-8)^2 - (m-8)^2 + (k-8)^2 \\ (n-8)^2 - (m-8)^2 - (k-8)^2 \end{matrix}\right\} d_2. \end{aligned} \tag{B9}$$

single cosine term as a function of d_0 and d_1 plus a constant term which is a function of d_2, i.e.,

$$P_2 = A_2 + B_2 \cos[2d_0 - 16d_1 + C_2(d_2)] \tag{B7}$$

where A_2 and B_2 are generally functions of d_2.

For the third-order distortion power, we follow a similar argument and apply it to the third-order distortion voltage given in (3). Assume that the frequency components of interest are specified at $\omega = K\omega_s$, $K = K_1, K_2, \cdots, K_M$. Then similar to P_2 in (B3), the third-order distortion power is given by

$$\begin{aligned} P_3 = &\frac{1}{2} \sum_{n \pm m \pm k = K_1} A_{nmk}^2 \\ &+ \frac{1}{2} \sum_{n \pm m \pm k = K_2} A_{nmk}^2 + \cdots \\ &+ \frac{1}{2} \sum_{n \pm m \pm k = K_M} A_{nmk}^2 \\ &+ \sum_{\substack{i \\ (i \neq j)}} \sum_j A_{K_1,i} A_{K_1,j} \\ &\cdot \cos[\phi_{n \pm m \pm k = K_1, i} - \phi_{n \pm m \pm k = K_1, j}] \\ &+ \sum_{\substack{i \\ (i \neq j)}} \sum_j A_{K_2,i} A_{K_2,j} \\ &\cdot \cos[\phi_{n \pm m \pm k = K_2, i} - \phi_{n \pm m \pm k = K_2, j}] \\ &+ \cdots + \sum_{\substack{i \\ (i \neq j)}} \sum_j A_{K_M,i} A_{K_M,j} \\ &\cdot \cos[\phi_{n \pm m \pm k = K_M, i} - \phi_{n \pm m \pm k = K_M, j}] \end{aligned} \tag{B8}$$

where $A_{K,i} \equiv A_{nmk} = \beta a_n a_m a_k$ with $n \pm m \pm k = K$ and i denotes the distinct set of (n, m, k), and $\phi_{n \pm m \pm k = K, i} \equiv \phi_n \pm \phi_m \pm \phi_k$ with $n \pm m \pm k = K$ and the corresponding ith distinct (n, m, k) set. The constant factor β is equal to $\frac{3}{2}$, or $\frac{3}{4}$ or $\frac{1}{4}$, depending on the type of the third-order distortion product, as shown in (3). Applying the quadratic-phase relationship of (B4) to $\phi_n \pm \phi_m \pm \phi_k$, we obtain (B9), shown at the top of the page. Substituting (B9) into (B8), we observe that a typical cosine term inside the second bracket is either of the form

$$\cos[4d_0 - 32d_1 + d_2 \cdot \text{function of } (n, m, k)] \tag{B10a}$$

$$\cos[2d_0 - 16d_1 + d_2 \cdot \text{function of } (n, m, k)] \tag{B10b}$$

$$\cos[d_2 \cdot \text{function of } (n, m, k)] \tag{B10c}$$

which is also periodic in d_0 and d_1. However, if (B8) contains both terms involving cosine of $[4d_0 - 32d_1]$ and cosine of $[2d_0 - 16d_1]$, then (B8) no longer can be combined as a single cosine term as in (B7), but is of the form

$$\begin{aligned} P_3 = A_3 &+ B_3 \cos[2d_0 - 16d_1 + C_3(d_2)] \\ &+ D_3 \cos[4d_0 - 32d_1 + E_3(d_2)] \end{aligned} \tag{B11}$$

where A_3, B_3, and D_3 are generally functions of d_2. We see that (B11) is periodic in d_0 and d_1 with the period equal to π for d_0 and the period of $2\pi/16$ for d_1, but is not a cosine waveform (with respect to the arguments d_0 and d_1), unless D_3 is identically zero.

From (B9), it is clear that D_3 will be zero (i.e., no cosine of $[4d_0 - 32d_1]$ term) if there is no third-order distortion product of the type $(n - m - k)$. In our CATV application, the frequency band above the analog-carrier band is of interest for digital transmission. Over this band, there will be no third-order distortion product of the type $(n - m - k)$. Therefore, with D_3 equal to zero, (B11) of P_3 is the same form as (B7) of P_2. Both equations then prescribe an ellipse in the parametric plot of P_2 versus P_3 as d_0 or d_1 is varied over a period. Since the argument of the cosine is $[2d_0 - 16d_1]$ for both P_2 and P_3, one can fix the value of d_0 and trace the same ellipse by varying d_1 or vice versa. In any case, (B7) and (B11) together prescribes a closed curve in the parametric plot of P_2 versus P_3, which is generally elliptical, since in practice there are many more third-order distortion products of the types $n + m + k$ and $n + m - k$ combined than those of the type $n - m - k$, resulting in D_3 much smaller than B_3.

Using similar arguments, it can be shown that parametric plots of the peak/rms ratio (or more precisely the (peak/rms)^2) plotted against P_2 or P_3 also form closed contours with the period in d_1 equal to $2\pi/16$.

References

[1] I. Switzer, "A harmonically related carrier system for cable television," *IEEE Trans. Commun.*, vol. COM-23, pp. 155–166, Jan. 1975.

[2] W. Krick, "Improvement of CATV transmission using an optimum coherent carrier system," *IEEE Trans. Cable Television*, vol. CATV-5, pp. 65–71, Apr. 1980.

[3] F. J. Effenberger, "Efficient optical transmission of NTSC video," in *12th Annual Nat. Fiber Opt. Eng. Conf., Session 6*, Denver, CO, Sept. 1996, pp. 311–322.

[4] C. E. Cook and M. Bernfeld, *Radar Signals.* New York: Academic, 1967.

[5] M. R. Schroeder, "Synthesis of low-peak-factor signals and binary sequences with low autocorrelation," *IEEE Trans. Inform. Theory*, vol. IT-16, pp. 85–89, Jan. 1970.

[6] S. Boyd, "Multitone signals with low crest factor," *IEEE Trans. Circuits Syst.,* vol. CAS-83, pp. 1018–1022, Oct. 1986.
[7] D. R. Gimlin and C. R. Patisaul, "On minimizing the peak-to-average power ratio for the sum of N sinusoids," *IEEE Trans. Commun.,* vol. 41, pp. 631–635, Apr. 1993.
[8] N. M. Blachman, *Noise and Its Effect on Communication,* 2nd ed. New York: Krieger, 1982.
[9] A. Papoulis, *Signal Analysis.* New York: McGraw-Hill, 1977.
[10] W. R. Bennett, "Distribution of the sum of randomly phased components," *Q. Appl. Math.,* pp. 385–393, Jan. 1948.
[11] C. Bianchi, G. Lentz, and R. Welter, "Performance of QAM on a hybrid fiber-coax system," in *49th ARFTG Conf. Dig.,* Denver, CO, June 1997, pp. 24–33.

Gary D. Alley (S'70–M'72–SM'82) was born in Kansas City, MO, on August 12, 1943. He received the B.S., M.S., and Ph.D. degrees in electrical engineering from the University of Kansas, Lawrence, in 1966, 1967, and 1972, respectively.

In 1967, he joined Bell Telephone Laboratories, Whippany, NJ, as Technical Staff Member, where he was engaged in the design of microwave integrated circuits. From 1970 to 1972, he was at the University of Kansas, on leave of absence from Bell Laboratories, where he conducted theoretical studies of microwave field-effect transistors. In July 1972, he returned to Bell Laboratories, North Andover, MA, where he was involved in the design of microwave circuits for communication systems. In 1978, he joined the staff of the solid-state division of MIT Lincoln Laboratories where he worked on the design of GaAs microwave devices. In February of 1982, he returned to Bell Laboratories, where he has been involved in microwave circuit design, analysis of hybrid fiber-coaxial systems, equalization of 10-Gb/s optical systems, and has supervised a group responsible for a wide variety of microwave radio systems work. He has published or presented over 30 papers on microwave circuits, semiconductor devices, and microwave radio propagation.

Dr. Alley is a member of Tau Beta Pi and Eta Kappa Nu. He was co-recipient of the 1982 W. R. G. Baker Prize Award from the IEEE Board of Directors, for a paper which appeared in the IEEE TRANSACTIONS ON ELECTRON DEVICES.

Yen Long Kuo (S'61–M'66–SM'80–F'82) was born on November 18, 1936. He received the diploma degree from the Taipei Institute of Technology, Taipei, Taiwan, R.O.C., in 1957, the M.S. degree from Oklahoma State University, Norman, in 1961, and the Ph.D. degree from the University of California at Berkeley, in 1966, all in electrical engineering.

From 1970 to 1996, he was a Distinguished Technical Staff Member at AT&T Bell Laboratories. His work experience included system analysis and system engineering for the HFC-2000 Hybrid Fiber Coax System, design of 622-MHz SAW-based VCO, design of 155-MHz bipolar chips for timing recovery circuits, design of the D4/D5 automatic equalizer, 16-QAM adaptive equalizer design for digital transmission systems, development of CAD analysis tools for capacitor circuits design, and the development of CAD tools for intermodulation distortion analysis of analog transmission systems. In 1981, he was a Visiting Professor at National Taiwan Institute of Technology, Taipei, Taiwan, R.O.C. while on leave from AT&T Bell Laboratories. From 1966 to 1970, he was an Assistant Professor at Purdue University, Lafayette, IN. From 1965 to 1966, he was an Acting Assistant Professor at the University of California at Berkeley. He has authored or co-authored over 10 papers in refereed journals and numerous conference papers.

Dr. Kuo was an associate editor of the IEEE TRANSACTIONS ON CIRCUITS AND SYSTEMS from 1977 to 1979. From 1982 to 1985, he was a member of the IEEE Circuits and Systems Society Administration Committee. From 1987 to 1989, he was Editor-in-Chief of the IEEE TRANSACTIONS ON CIRCUITS AND SYSTEMS. He received the AT&T Bell Laboratories Fellow Award for "Contribution to the Design of Digital Transmission Systems, including the Invention of D5 Data Port Multi-Rate Equalizer" in 1986, the IEEE Fellow Award for "Contribution to the Computer-Aided Analysis and Design of Communication Circuits" in 1982, and the IEEE Circuits and Systems Society's Darlington Best Paper Award in 1975 for "Distortion Analysis of Bipolar Transistor Circuits," published in the IEEE TRANSACTIONS ON CIRCUIT THEORY, November 1973.